

The Hemiplegic Migraine associated Y1245C mutation in the III-S1 segment of CACNA1A results in a gain of channel function due to its effect on the voltage sensor.

Abbreviated Title: CPS and HM mutation affects Cav2.1 voltage sensor function.

Selma A. Serra¹, Noelia Fernández-Castillo², Alfons Macaya³, Bru Cormand^{2,4,5}, Miguel A. Valverde¹ and José M. Fernández-Fernández¹.

¹ Laboratory of Molecular Physiology and Channelopathies, Department of Experimental and Health Sciences, Universitat Pompeu Fabra, PRBB, C/ Dr. Aiguader 88, 08003 Barcelona, Spain;

²Departament de Genètica, Universitat de Barcelona, Barcelona, Spain;

³Laboratori de Neurobiologia Cel·lular i Molecular, Departament de Patologia i Terapèutica Experimental, Facultat de Medicina, Institut d'Investigacions Biomèdiques de Bellvitge-Universitat de Barcelona, Barcelona, Spain;

⁴Centro de Investigación Biomédica en Red de Enfermedades Raras (CIBERER), Barcelona, Spain and ⁵Institut de Biomedicina de la Universitat de Barcelona, Barcelona, Spain.

Correspondence should be addressed to José M. Fernández-Fernández, PhD, Laboratory of Molecular Physiology and Channelopathies, Department of Experimental and Health Sciences, Universitat Pompeu Fabra, PRBB, Room 331.02, C/ Dr. Aiguader 88, 08003 Barcelona, Spain. Phone: 34 93 3160851 Fax: 34 93 3160901; Email: jmanuel.fernandez@upf.edu

Keywords: P/Q calcium channel; voltage sensor S1 segment; G β γ -mediated inhibition; Benign Paroxysmal Torticollis of Infancy; Benign Paroxysmal Vertigo of Childhood; Hemiplegic Migraine.

Abstract

Mutations in the gene encoding the pore-forming $\alpha 1A$ subunit of P/Q Ca^{2+} channels (CACNA1A) are linked to familial hemiplegic migraine. CACNA1A Y1245C is the first missense mutation described in a subject affected with childhood periodic syndromes that evolved into hemiplegic migraine. Y1245C is also the first amino acid change described in any S1 segment of CACNA1A in a hemiplegic migraine background. We found that Y1245C induced a 9- mV left shift in the current-voltage activation curve, accelerated activation kinetics, and slowed deactivation kinetics within a wide range of voltage depolarizations. Y1245C also left-shifted the voltage-dependent steady-state inactivation with a significant increase in steepness, suggesting a direct effect on the P/Q channel voltage sensor. Moreover, Y1245C reduced $G\beta\gamma$ subunits-dependent channel inhibition probably by favoring $G\beta\gamma$ dissociation from the channel; an effect also observed using actionpotential-like waveforms of different durations. The formation of a new disulfide bridge between cysteines may contribute to the Y1245C effects on activation and $G\beta\gamma$ inhibition of the channel, as they were significantly reversed by the sulphhydryl-reducing agent dithiothreitol. Together, our data suggest that Y1245C alters the structure of the $\alpha 1A$ voltage sensor producing an overall gain of channel function that may explain the observed clinical phenotypes.

Introduction

Several mutations in the CACNA1A gene, encoding the P/Q Ca^{2+} channel $\alpha 1$ subunit ($\alpha 1A$), have been linked to familial hemiplegic migraine (FHM), an autosomal dominantly inherited subtype of migraine with aura that also features some degree of transient hemiparesis [26]. P/Q Ca^{2+} channels are expressed in the brain areas involved in the pathogenesis of migraine including nociceptive pathways [26] and are localized at presynaptic terminals [31] tightly coupled to neurotransmitter release [5].

The $\alpha 1A$ subunit consists of four repeated domains (I- IV) each containing six transmembrane regions (S1-S6) with a voltage sensor (S1-S4) and a pore loop between S5 and S6. Multiple regulatory proteins interact with $\alpha 1A$ modulating its inherent activation/inactivation properties [5]. A major modulation of voltage-dependent P/Q Ca^{2+}

channels, with high relevance in the control of synaptic transmission, occurs via the receptor-triggered release of G proteins $\beta\gamma$ ($G\beta\gamma$) subunits. $G\beta\gamma$ dimers bind to multiple regions on the $\alpha 1A$ subunit to produce membranedelimited voltage-dependent inhibition of the Ca^{2+} channel [9]. Inhibited channels activate at more depolarized voltages and with slower kinetics, due to a restricted movement of the voltage sensor that makes the channel more reluctant to open [18]. A key feature of this inhibition involves the dissociation of $G\beta\gamma$ subunits as channels undergo conformational changes in response to strong depolarization, leading to the facilitation of Ca^{2+} currents [9].

Mutations in *CACNA1A* underlying FHM are mainly found around the line pore (S5-P-S6 segments), in the loops connecting S3-S4 or S4-S5 segments and in the S4 segment of the voltage sensors [26]. Functional analysis of disease-causing mutations in heterologous expression systems and neurons from FHM knockin mice revealed an overall gain of P/Q channel function that favored initiation and propagation of cortical spreading depression (CSD), the electrophysiological correlate of the aura [reviewed in 26]. According to the International Headache Society, several Childhood Periodic Syndromes (CPS) are considered precursors of migraine in young patients, including cyclic vomiting, abdominal migraine and benign paroxysmal vertigo of childhood (BPV). Although benign paroxysmal torticollis of infancy (BPT) is not yet included in this classification, different reports suggest that it might be the earliest manifestation of migraine in life, with a possible genetic linkage to *CACNA1A* mutations in a hemiplegic migraine background [7, 15]. The Y1245C mutation in the III-S1 segment of $\alpha 1A$ has been the first nonsynonymous variation proposed as pathogenic in a patient affected with CPS, who displayed a changing, age-specific phenotype beginning as BPT, evolving into BPV and later becoming hemiplegic migraine (HM) [7]. We now report that Y1245C, the first amino acid change described in the S1 segment of any $\alpha 1A$ domain in a patient with HM, affects the function of the voltage sensor and lessens $G\beta\gamma$ -mediated inhibition resulting in gain of channel function, thereby supporting mutation pathogenicity.

Materials and methods

DNA constructs and site-directed mutagenesis

cDNAs of the $\alpha 1A$ and $\alpha 2\delta$ subunits of the *CaV2.1* neuronal calcium channel were obtained from rabbit (rabbit BI-1 subunit is highly homologous to human $\alpha 1A$ subunit [22]), and the *CaV β 2a* was from rat. P/Q channel formed by subunits from different species has been

reported to be fully functional and very similar to human P/Q channel [3]. The Y1245C mutation was introduced using the QuickChange™ Site-Directed Mutagenesis XL kit (Stratagene, La Jolla, CA) and the primers 5′ -CCTGAACCTGCGCTGCT TCGAGATGTGCAT-3′ (sense) and 5′ -ATGCACATCTC GAAGCAGCGCAGGTTTCAGG-3′ (antisense). All cDNA clones were sequenced in full to confirm their integrity and transferred to the pcDNA3 vector for subsequent transfection in HEK 293 cells.

Heterologous expression and electrophysiology

HEK 293 cells were transfected using a linear polyethylenimine (PEI) derivative, the polycation ExGen500 (Fermentas Inc., Hanover, Maryland, USA) as previously reported (eight equivalents PEI/3.3 µg DNA/dish) [13]. Transfection was performed using the ratio for α1A (WT or Y1245C), CaVβ2a, α2δ, and EGFP (transfection marker) of 1:1:1:0.3. In some experiments G protein β1 and γ2 subunits were also transfected at the same ratio as P/Q channel subunit cDNAs. Recordings were done 24-72 h after transfection.

Calcium currents (I_{Ca}) through wild-type (WT) or Y1245C P/Q channels were measured using the whole-cell configuration of the patch-clamp technique [17]. Pipettes had a resistance of 2-3 MΩ when filled with a solution containing (in mM): 140 CsCl, 1 EGTA, 4 Na₂ATP, 0.1 Na₃GTP, and 10 Hepes (pH 7.2-7.3 and 295-300 mosmol/l). The external solution contained (in mM): 140 tetraethylammonium-Cl, 3 CsCl, 2.5 CaCl₂, 1.2 MgCl₂, 10 Hepes, and 10 glucose (pH 7.3-7.4 and 300-305 mosmol/l). When measuring Ca²⁺ currents elicited by action-potential-like waveforms (APWs), the extracellular [Ca²⁺] employed was 5 mM in order to favor Ca²⁺ entry, particularly in response to fast APW in the presence of Gβγ subunits. Recordings were obtained with a D-6100 Darmstadt amplifier (List Medical, Germany), filtered at 1 kHz (only for short (millisecond) pulses) and corrected for leak and capacitive currents using the leak subtraction procedure (P/8 for short pulses and P/4 for long (second) pulses). Currents were acquired at 33 kHz (for short pulses) or 5 kHz (for long pulses). The pClamp8 software (Axon Instruments, Foster City, CA, USA) was used for pulse generation, data acquisition and subsequent analysis.

Peak inward Ca²⁺ currents were measured from cells clamped at -80 mV and pulsed for 20 ms from -60 mV to +70 mV in 5 mV steps. A modified Boltzmann equation (Eq. 1) was fitted to normalized current-voltage (I-V) to obtain the voltage-dependence of activation,

$$I = G_{\max} (V - V_{\text{rev}}) / (1 + \exp(-(V - V_{1/2,\text{act}}) / k_{\text{act}})) \quad (1)$$

Time constant for activation (τ_{act}), deactivation (τ_{deact}), and inactivation (τ_{inact}) were obtained from single exponential fits of I_{Ca} activation phase, tail currents obtained with 20-ms prepulse to +20 mV (to maximally open the voltage-gated P/Q channels) and followed by test pulses between -80 and +10 mV (in 5 mV steps) for 30 ms and the inactivation phase of I_{Ca} during a 3 s pulse from a holding potential of -80 mV to a test potential of +20 mV, respectively.

Time course of I_{Ca} recovery from inactivation ($\tau_{reïnact}$) was tested applying a second pulse of 50 ms to +20 mV at increasing time intervals (1-106 s) after the inactivating prepulse. Normalized peak I_{Ca} at different times was fitted to a single exponential.

The voltage-dependence of steady-state inactivation was estimated by measuring peak I_{Ca} currents at +20 mV following 30 s steps to various holding potentials (conditioning pulses) between -100 and +10 mV (Fig. 3c). During the time interval between test pulses (20 ms) cells were held at -80 mV. I_{Ca} currents obtained following the conditioning pulses were normalized to maximal I_{Ca} to determine the persistent current. Half-maximal voltage ($V_{1/2, inact}$) and slope factor for steady-state inactivation (k_{inact}) were obtained by fitting the data to the following Boltzmann equation (Eq. 2),

$$I/I_{max} = 1 / (1 + \exp((V - V_{1/2, inact}) / k_{inact})) \quad (2)$$

The voltage-dependence of ICa inhibition by G β 1 γ 2 subunits was examined by applying a family of 20-ms pulses to various voltages (between -60 mV and +70 mV in 5 mV steps) 10 ms before (P1) and 1 ms after (P2) a 50-ms conditioning prepulse to +100 mV (PP), from a holding potential of -80 mV. Facilitation at different voltages was then determined as the ratio ICa(P2/P1). Ca²⁺ current facilitation was also evaluated by applying a 20-ms test pulse to +20 mV before and 1 ms after a train of 15 4-ms square steps to +30 mV or +100 mV, delivered at a frequency of 71.4 Hz (i.e., time between pulses in the train was 10 ms; holding potential was -80 mV).

Facilitation decay (G β γ association to the P/Q channel) was studied by using a three-pulse voltage protocol consisting of two 20-ms test pulses (P1 and P2) to +20 mV separated by a conditioning prepulse to +100 mV (PP), and varying the time between PP and P2 (from 1 to 60 ms; Fig. 6a). Facilitation development (G β γ dissociation from the P/Q channel) was studied by using a similar three-pulse voltage protocol applying different voltages for the conditioning prepulse (+100 mV, +50 mV, +30 mV, and +10 mV) and incrementing its

duration from 0 to 70 ms (Fig. 7a). Plots of $I_{Ca}(P2/P1)$ as a function of Δt were fitted to single exponentials in order to obtain the corresponding time constants (τ_{decay} and $\tau_{development}$).

Ca^{2+} entry through WT and Y1245C P/Q channels in the absence and presence of $G\beta 1\gamma 2$ dimers was also measured in response to three different action-potential-like waveforms (APWs) that have been reported to represent a wide range of action-potential durations present in neurons [25]. Briefly, the duration at half-amplitude and the rising phase slope were, respectively: 0.5 ms and 300 mV/ms for the fast APW, 1 ms and 94 mV/ms for the medium APW and 2.2 ms and 85 mV/ms for the slow APW. All APWs were normalized to a resting potential of -60 mV and a peak amplitude of $+30$ mV (Fig. 8a) (removal of the AP afterhyperpolarization phase does not affect significantly the evoked Ca^{2+} current [25]). Ca^{2+} currents were acquired at 33 kHz and an average of four to six traces were used for all comparisons. The total Ca^{2+} influx (QCa) evoked by the APWs was measured as the integral of the Ca^{2+} current delimited by the time point at which inward current initially diverged from the baseline, and the time at which it returned to baseline.

All experiments were carried out at room temperature ($22-24^{\circ}C$).

Statistics

Data are presented as the means \pm S.E.M. Statistical tests included Student's *t* test, Mann-Whitney test, One-way analysis of variance (ANOVA) followed by a Bonferroni post-hoc test, or nonparametric ANOVA (Kruskal-Wallis Test) followed by Dunn post-hoc test, as appropriate. Differences were considered significant if $P < 0.05$.

Results

Current density and activation/inactivation properties of heterologously expressed WT and Y1245C P/Q channels

Y1245C is located in a highly conserved and functionally important region of the human $\alpha 1A$ subunit of neuronal P/Q-type Ca^{2+} channels (Fig. 1). It lies in the S1 segment of domain III (III-S1; at the interface of the first transmembrane region and the cell cytoplasm), which forms part of the voltage sensor [27]. Maximum current densities resulting from expression of mutant Y1245C $\alpha 1A$ ($\alpha 1A(Y1245C)$) were comparable to current densities of wild-type (WT) $\alpha 1A$ channels ($P=0.63$; Fig. 2a and c, left panel). The potential for half-maximal activation ($V_{1/2, act}$) was significantly ($P < 0.0001$) shifted to hyperpolarized potentials for Y1245C channels (by ~ 9 mV), without changing the steepness of the activation curve (k_{act})

or the apparent reversal potential (V_{rev} ; ruling out major changes in Ca^{2+} permeability; Fig. 2c, right panel). Consistently, the maximum current amplitude was elicited by depolarizing pulses to +20 mV or +10 mV for WT or Y1245C channels, respectively (Fig. 2c). Activation and deactivation kinetics were also left-shifted in the Y1245C channel (Fig. 2d and e, respectively). Thus, the highest τ_{act} for WT (2.22 ± 0.1 ms, $n=61$) or Y1245C (2.08 ± 0.1 ms, $n=33$) I_{Ca} were observed at +10 mV and 0 mV, respectively. Furthermore, activation kinetics of $\alpha 1A(Y1245C)$ channels were significantly accelerated ($P < 0.01$) in a wide range of depolarizing voltages (from +5 to +50 mV), when compared to $\alpha 1AWT$ channels (Fig. 2a and d). $\alpha 1A(Y1245C)$ channels also presented slower τ_{deact} ($P < 0.05$) at voltages from -30 to 0 mV (Fig. 2b and e).

To investigate whether the Y1245C mutation affects the time course of channel inactivation, we analyzed I_{Ca} decay during a 3-s test pulse elicited from a holding potential of -80 mV to +20 mV (Fig. 3a). No significant differences between WT and Y1245C channels were observed ($P = 0.17$). The rate of recovery from inactivation was also unaffected in Y1245C channels (Fig. 3b, $P = 0.5$). Nevertheless, the half-maximal voltage for steady-state inactivation ($V_{1/2, inact}$) induced by 30-s conditioning prepulses between -100 and +10 mV (Fig. 3c, top panel) was leftshifted (~ 15 mV) in Y1245C channels ($P < 0.0001$). Such effect was accompanied by a significant ($P < 0.05$) increase in the steepness of the inactivation curve (symbolized by k_{inact} ; Fig. 3c and d). Alterations in the steady-state inactivation parameters without changes in inactivation kinetics have been previously reported for several FHMcausing CACNA1A mutations [23].

Effect of Y1245C on voltage-dependent $G\beta\gamma$ -mediated inhibition of P/Q Ca^{2+} channels

Co-expression of $\alpha 1AWT$ or $\alpha 1A(Y1245C)$ together with $\beta 2a$ and $\alpha 2\delta$ subunits and G protein $\beta 1\gamma 2$ dimers in HEK 293 cells resulted in current facilitation (larger and faster P2 than P1 currents following a 50-ms prepulse (PP) to +100 mV), reflecting the voltage-dependent relief of $G\beta\gamma$ -mediated channel inhibition (Fig 4a). In the absence of $G\beta 1\gamma 2$, no basal facilitation was observed (no difference between P1 and P2; mean facilitation ratio at +20 mV was 0.99 ± 0.008 ($n=10$) for WT and 0.99 ± 0.01 ($n=10$) for Y1245C channels), indicative of no tonic channel inhibition by endogenous G protein subunits. Full averaged I-V curves before and after PP, normalized to the peak I_{Ca} obtained at P1, are shown in Fig. 4b. Both WT and Y1245C channels are inhibited by overexpressed $G\beta 1\gamma 2$ within a voltage range from -10 to +35 mV. Current facilitation, due to the dissociation of $G\beta\gamma$ dimers from the channels after strong depolarization, produced a significant shift in the voltage-dependent activation

to more hyperpolarized voltages for both WT and Y1245C channels (~ 6 mV, $P < 0.001$). Interestingly, mean facilitation ratio ($P2/P1$) was significantly reduced by the Y1245C mutation at test potentials ranging from +5 to +20 mV (Fig. 4a, b and c). This result, together with the observation that both WT and Y1245C facilitated ($P2$) currents are of similar magnitude to the corresponding currents recorded in the absence of $G\beta 1\gamma 2$ (compare black columns in Fig. 4d with Fig. 2c), reflect a lower level of $G\beta\gamma$ -mediated inhibition in mutant channels (estimated from $P1$ and $P2$ Fig. 2). Y1245C affects activation and deactivation properties of heterologously expressed P/Q channels. a Current traces illustrating voltage-dependence and activation kinetics of WT (top) and Y1245C (bottom) channels, in response to 20 ms voltage pulses. b Current traces illustrating deactivation kinetics of WT (top) and Y1245C (bottom) channels obtained by hyperpolarizing the cells during 30 ms at the indicated voltages following a 20-ms depolarizing pulse to +20 mV. Dotted lines in the current traces indicate the zero current level. c Current density-voltage relationships (left panels) and normalized I-V curves (right panels) for WT (empty circle, $n=71$) and Y1245C P/Q (filled circle, $n=34$) channels expressed in HEK 293 cells. $V_{1/2, act}$, k_{act} and V_{rev} values were (in mV): WT (empty circle, $n=71$) 7.55 ± 0.44 , 3.93 ± 0.33 and 64.35 ± 0.83 ; Y1245C (filled circle, $n=34$) -1.48 ± 0.56 , 3.72 ± 0.44 and 61.56 ± 1.13 , respectively. Average τ_{act} and τ_{deact} of WT (empty circle) and Y1245C channels (filled circle) at the indicated voltages current density values, Fig. 4d). Similar results were obtained using, instead of the long-lasting pulse to +100 mV, a more physiological stimulation with trains of short depolarizing pulses delivered at 71.4 Hz (Fig. 5). WT P/Q currents were facilitated when cells were stimulated by trains of pulses to +30 and +100 mV (Fig. 5a (top) and b) while Y1245C currents only showed facilitation (although smaller than WT channels) during the train to +100 mV (Fig. 5a (bottom) and b).

We also evaluated time courses for re-inhibition (at -80 mV) following facilitatory depolarization (facilitation decay) and for relief from inhibition (at +100 mV; facilitation development), reflecting the association and dissociation rates of $G\beta\gamma$ dimers to/from the channel, physiological voltages as has been recently suggested for other two FHM mutations [30]. Therefore, we assessed facilitation development kinetics at lower-conditioning prepulse voltages that were able to render current facilitation (+50, +30, and +10 mV). Y1245C significantly accelerated the dissociation of $G\beta\gamma$ from P/Q channels at lower depolarizing voltages (+10 to +30 mV; Fig. 7b, c, d (left panels) and e).

Moreover, to gain insights into the physiological impact of the reduction in $G\beta\gamma$ -mediated voltage-dependent inhibition of the P/Q Ca^{2+} current due to the Y1245C mutation, we

measured the Ca²⁺ influx through WT and mutant channels elicited by single-action-potential-like waveforms (APWs) of different durations (fast, medium, and slow; Fig. 8a, top) in the absence and presence of Gβ1γ2. Overexpression of Gβ1γ2 dimers reduced both peak current density and total Ca²⁺ influx (QCa) through WT channels in response to APWs by ~89 and ~90 %, respectively. Interestingly, the Gβ1γ2-mediated reduction of both parameters in cells expressing Y1245C channels was lower: 62% (at fast APW) and 48% (at medium and slow APWs) for the peak current; 74% (at fast APW) and 50% (at medium and slow APWs) for QCa. Thus, in the presence of Gβ1γ2, Y1245C currents evoked by APWs were significantly larger than WT currents. Application of APWs in the absence of Gβ1γ2 to cells expressing Y1245C channels produced current density and QCa values that were always superior to those obtained from cells expressing WT channels, although significant differences were only observed when stimulating with fast APW (Fig. 8). No currents were detected in non-transfected HEK 293 cells in response to the three different APWs (data not shown). respectively. No significant differences between WT and Y1245C channels were observed regarding facilitation kinetics under the above-mentioned conditions (Fig. 6 and Fig. 7b, c, d (right panels) and e). However, these measurements at extreme voltages reflect, at best, the Gβγ association rate to the closed channel and the dissociation rate from the open channel, respectively, without addressing the effects of the mutation on the Gβγ dissociation rate from the channel at intermediate more physiological voltages as has been recently suggested for other two FHM mutations [30]. Therefore, we assessed facilitation development kinetics at lower-conditioning prepulse voltages that were able to render current facilitation (+50, +30, and +10 mV). Y1245C significantly accelerated the dissociation of Gβγ from P/Q channels at lower depolarizing voltages (+10 to +30 mV; Fig. 7b, c, d (left panels) and e). Moreover, to gain insights into the physiological impact of the reduction in Gβγ-mediated voltage-dependent inhibition of the P/Q Ca²⁺ current due to the Y1245C mutation, we measured the Ca²⁺ influx through WT and mutant channels elicited by single-action-potential-like waveforms (APWs) of different durations (fast, medium, and slow; Fig. 8a, top) in the absence and presence of Gβ1γ2. Overexpression of Gβ1γ2 dimers reduced both peak current density and total Ca²⁺ influx (QCa) through WT channels in response to APWs by ~89 and ~90 %, respectively. Interestingly, the Gβ1γ2-mediated reduction of both parameters in cells expressing Y1245C channels was lower: 62% (at fast APW) and 48% (at medium and slow APWs) for the peak current; 74% (at fast APW) and 50% (at medium and slow APWs) for QCa. Thus, in the presence of Gβ1γ2, Y1245C currents evoked by APWs were significantly larger than WT currents. Application of APWs in the absence of Gβ1γ2 to cells expressing Y1245C channels produced current density and QCa

values that were always superior to those obtained from cells expressing WT channels, although significant differences were only observed when stimulating with fast APW (Fig. 8). No currents were detected in non-transfected HEK 293 cells in response to the three different APWs (data not shown).

DTT lessens the effects of the Y1245C mutation on activation and Gβγ inhibition of the P/Q channel

Because disulfide bridges among cysteine residues generally play an important role in stabilizing a protein's threedimensional structure, we hypothesized that the cysteine insertion, due to the Y1245C mutation, results in a conformational change of the III-S1 segment affecting voltage-sensor function, channel-gating and, in turn, modulation of channel activity by Gβγ (since these G protein subunits act on voltage-dependent Ca²⁺ channels by inhibiting voltage sensor movement [18]). Therefore, we tested the effects of breaking disulfide bridges with the sulphhydryl-reducing agent dithiothreitol (DTT) on activation properties and current facilitation following strong depolarization in the presence of Gβ1γ2 dimers of both WT and Y1245C currents. As expected, this new set of experiments reported a significant left shift in both the voltage-dependent activation (~8 mV) and activation kinetics (Fig. 9a, b and c, left panels) for Y1245C channels when compared to WT before DTT application. Exposure to 1 mM DTT had no significant effect on the activation voltage-dependence or activation kinetics of WT channels, ruling out the involvement of a disulfide bridge in the voltage-dependent gating of WT P/Q channels, but significantly shifted both parameters to more depolarized potentials in the case of Y1245C channels. Thus, DTT right-shifted V_{1/2, act} of mutant channels by ~4 mV (P< 0.0001), although did not fully recover the values obtained with WT channels (P<0.0001; Fig. 9a and b, right panels). DTT reversed in full the differences in τ_{act} between WT and Y1245C channels (Fig. 9a and c, right panels). No differences between WT and Y1245C were observed regarding k_{act} or V_{rev} which were similar under all experimental conditions. DTT exposure also reversed Y1245C-induced decrease in current facilitation without significantly affecting WT current facilitation (Fig. 10). Altogether, these results suggest that mutation Y1245C improves P/Q channel activity mainly due to the formation of a new disulfide bridge among cysteines.

Discussion

We have recently described the presence of the Y1245C mutation in the III-S1 segment of the P/Q Ca²⁺ channel α1 subunit (CACNA1A) in a patient that presented benign paroxysmal torticollis of infancy (BPT) during the neonatal period. This clinical phenotype evolved with

aging, first to benign paroxysmal vertigo of childhood (BPV) and then to hemiplegic migraine (HM) [7]. This sequence of the changing, age-specific clinical phenotypes has been suggested for other patients [10, 11]. Y1245C is the first reported mutation in the S1 segment of any domain of the $\alpha 1A$ subunit in any patient with HM. This residue is highly conserved in evolution at the interspecies level as well as among the CaV2 family of human calcium channels (Fig. 1), indicating functional and/or structural relevance. In order to properly establish the pathogenicity of the Y1245C mutation, we have studied its functional consequences on P/Q channels expressed in HEK 293 cells. Our data show that mutation Y1245C affects different biophysical properties of P/Q channels: (1) shifts current activation curve to lower voltages (~ 9 mV), an effect that may account for the increased current density and Ca^{2+} influx through Y1245C channels in response to APWs when compared with WT channels (Fig. 8) and, therefore, may translate into an augmented exocytosis due to the non-linear relationship between Ca^{2+} influx and the triggering of this secretory process [8]; (2) accelerates activation kinetics and slows deactivation kinetics within a wide range of voltage depolarizations; and (3) shifts voltage-dependent steady-state inactivation to less depolarized voltages (~ 15 mV), an effect accompanied by a significant increase in steepness. We also found that mutation Y1245C accelerates $\text{G}\beta\gamma$ dissociation from the channel, an effect that can account for the reduced P/Q channel voltage-dependent inhibition by $\text{G}\beta\gamma$ subunits at voltages that may be attained during CSD. Moreover, the reduction in $\text{G}\beta\gamma$ -mediated inhibitory pathway induced by this mutation is also relevant under physiological conditions, as allows larger Ca^{2+} influx elicited by APWs of different durations. These results are consistent with a causative role of the Y1245C mutation in the disease.

A reduction in the voltage threshold of channel activation by ~ 10 mV (Y1245C induced a ~ 9 mV left shift) is a trait shared by all FHM-causing mutations in CACNA1A [28, 29, reviewed in 26]. Such gain of channel function favors CSD initiation and propagation in a FHM knockin mouse model [29]. CSD, an abnormal increase of cortical activity—followed by a long-lasting neuronal suppression wave—that propagates across the cortex, is thought to play a major pathophysiological role in migraine: it causes the aura and activates the trigeminovascular system evoking alterations in the meningeal blood vessels and brainstem nuclei that lead to the development of headache [1]. Although the molecular mechanisms initiating CSD are not fully understood, a positive feedback mechanism involving increased depolarization, extracellular K^+ concentration and glutamatergic neurotransmission in which P/Q Ca^{2+} channels play a pivotal role, appears crucial for triggering CSD [26].

CSD generation may be further facilitated by the reduction in the Gβγ-mediated inhibition observed for Y1245C mutant P/Q channels, which might increase Ca²⁺ influx into the presynaptic terminal promoting neurotransmitter release and contributing to a persistent state of hyperexcitability under certain conditions. Consistent with this hypothesis, a decrease in the direct inhibitory pathway carried by Gβγ following G-protein-coupled receptor stimulation has been previously reported for other two FHM mutations expressed in HEK 293 cells: R192Q and S218L, localized in the first domain of the α1A subunit at the S4 segment and the S4-S5 linker, respectively [21, 30].

However, an apparent controversy concerning the mechanism by which those FHM mutations reduce G protein inhibition of P/Q channels arise from these reports. Initially, it was proposed that R192Q mutation might modify the molecular mechanisms by which Gβγ dimers association to α1A alter voltage sensor movement in response to membrane potential changes but without affecting binding or unbinding rates [21]. Recently, a more detailed study has shown that these FHM mutations promote accelerated Gβγ dissociation from the activated channel in a range of low depolarizing voltages (−10 to +30 mV for S218L, and −10 to 0 mV for R192Q) without affecting the maximal Gprotein inhibition of P/Q channels measured at the start of the depolarization [30]. Nevertheless, such acceleration in Gβγ dissociation from the channels can contribute to the reduction in Gβγ-mediated inhibition and facilitation levels reported for the R192Q mutant. This reduction in Gβγ-mediated inhibition and facilitation was measured at 25 ms from the beginning of the test depolarizing pulses, time point where significant relief from inhibition may already have occurred giving the impression of reduced G protein inhibition for the mutant channel due to faster Gβγ dissociation [21, 30]. In agreement with this idea, we observed both, an acceleration in the rate of Gβγ dissociation and a decrease in the voltage-dependent current inhibition for Y1245C channels. We measured a decrease in the facilitation ratio at 20 ms from the beginning of the test depolarizing pulses, time point that allows greater recovery from Gβγ-mediated inhibition for mutant than for WT channels during P1 depolarization if faster Gβγ dissociation occurs. Furthermore, whereas overexpression of Gβγ subunits reduced Ca²⁺ entry through WT channels by ~90% during all APW tested, the degree of inhibition of Ca²⁺ entry through Y1245C channels was diminished at medium and slow APWs (50%) compared with fast APW (74%). These results can also be explained by a faster dissociation of Gβγ from the mutant channels during the depolarizing APW, becoming more evident with longer stimuli (medium and slow APWs).

Voltage-dependent inactivation of Ca²⁺ channels is also an important physiological mechanism regulating neurosecretion [2, 14]. Several FHM-causing CACNA1A mutations alter P/Q-type calcium channel inactivation [16, 19, 20, 23, 28, this report], underlining its physiological relevance. However, these changes are highly heterogeneous, involving both gain- and loss-of-function, and their contribution to the pathophysiology of the disease remains to be solved. Only for the FHM-causing S218L mutation has been suggested that the reduced extent of inactivation contributes to the severity of the associated clinical phenotype [28].

Most FHM-associated CACNA1A mutations produce substitutions of conserved amino acids in important functional regions, mainly including the pore lining, the loops connecting S3-S4 or S4-S5 segments and the S4 segment of the voltage sensors [26]. Mutation Y1245C produces functional changes similar to most FHM-causing mutations. The functional effects of reported FHM mutations are consistent with the implication of S4 segments in voltage-sensing and the driving of conformational alterations that open the channel's gate, and that the S4-S5 linker, the S5-S6 segments, and the P-loop play an important role in the gate conformation and/or the coupling between voltage-sensing and channel-gating [27]. Our results using the sulphhydryl-reducing agent DTT strongly suggest that the de novo appearance of a disulfide bridge among cysteines involving the III-S1 segment may result in a conformational change of the voltage sensor region affecting the movement of the S4 segment and/or channelgating, along with the regulation of both processes by Gβγ subunits in the Y1245C mutant channel. In this respect, it has been suggested that residues in the S1 segment may form part of a hydrophobic plug which constitutes the main energy barrier encountered by positively charged residues in S4 when they translocate during voltage-sensing [4]. At present, we have not been able to identify which of the multiple native cysteines of the α1A subunit is participating in the formation of the new disulfide bridge.

A still open question is how could the Y1245C mutation in the P/Q Ca²⁺ channel α1 subunit cause BPT and BPV? Although the etiopathogenesis of both paroxysmal syndromes is not well known, it has been suggested that these disorders may arise from a vestibular dysfunction due to CSD affecting cortical areas that process vestibular information [10, 24]. Therefore, the lower voltage threshold of activation and decreased inhibition by Gβγ dimers observed for the Y1245C mutant channel, which is expected to favor CSD triggering, may lead not only to HM but also to BPT and BPV syndromes. Further mechanistic insights into the pathophysiology of these childhood syndromes are needed in order to support such hypothesis. It is also unknown how a given mutation may be responsible of a variety of

clinical manifestations at different ages, although it might be related to a differential regulation of P/Q channel expression, function and/or subcellular targeting during brain development [6, 12].

In conclusion, this is the first functional characterization of a CACNA1A mutation found in a patient suffering childhood periodic syndromes (BPT and BPV) and HM. Our results suggest that mutation Y1245C causes a conformational change in the voltage sensor region (S1- S4) of the P/Q channel α 1 subunit which results in an overall gain of channel function that, by promoting CSD initiation and propagation, may underline the observed sequence of clinical phenotypes. Our data give further support to the validation of BPT as another childhood migraine equivalent.

Acknowledgments

We thank Dr. Lutz Birnbaumer for providing P/ Q channel cDNAs and Dr. Gemma Marfany for helpful suggestions on the DNA cloning experiments. Work funded by Fundació la Marató de TV3 (061331 to J.M.F-F and 061330 to B.C.), the Spanish Ministry of Science and Innovation (SAF2006-13893-C02-02 to J.M.F-F, SAF2006-13893-C02-01 to B.C., SAF2006-04973 to M.A.V., SAF2003-04704 to A.M.), Fondo de Investigación Sanitaria (red HERACLES RD06/0009 to M.A.V) and Generalitat de Catalunya (SGR05-848 to B.C. and SGR05-266 to M.A.V.); S.A.S. is a FPI grant holder from the Spanish Ministry of Science and Innovation; J.M.F-F is a Ramón y Cajal Fellow and M.A.V. is an ICREA Academia Fellow. The authors declare that they have no competing financial interests.

References

1. Bolay H, Reuter U, Dunn AK, Huang Z, Boas DA, Moskowitz MA (2002) Intrinsic brain activity triggers trigeminal meningeal afferents in a migraine model. *Nat Med* 8:136–142
2. Branchaw JL, Banks MI, Jackson MB (1997) Ca^{2+} - and voltage- dependent inactivation of Ca^{2+} channels in nerve terminals of the neurohypophysis. *J Neurosci* 17:5772–5781
3. Brodbeck J, Davies A, Courtney JM, Meir A, Balaguero N, Canti C, Moss FJ, Page KM, Pratt WS, Hunt SP, Barclay J, Rees M, Dolphin AC (2002) The ducky mutation in *Cacna2d2* results in altered Purkinje cell morphology and is associated with the

expression of a truncated $\alpha 2\Delta 2$ protein with abnormal function. *J Biol Chem* 277:7684–7693

4. Campos FV, Chanda B, Roux B, Bezanilla F (2007) Two atomic constraints unambiguously position the S4 segment relative to S1 and S2 segments in the closed state of Shaker K⁺ channel. *Proc Natl Acad Sci USA* 104:7904–7909
5. Catterall WA (2000) Structure and regulation of voltage-gated Ca²⁺ channels. *Annu Rev Cell Dev Biol* 16:521–555
6. Chang SY, Yong TF, Yu CY, Liang MC, Pletnikova O, Troncoso J, Burgunder JM, Soong TW (2007) Age and gender-dependent alternative splicing of P/Q-type calcium channel EF-hand. *Neuroscience* 145:1026–1036
7. Cuenca-León E, Corominas R, Fernández-Castillo N, Volpini V, del Toro M, Roig M, Macaya A, Cormand B (2008) Genetic analysis of 27 Spanish patients with hemiplegic migraine, basilar- type migraine and childhood periodic syndromes. *Cephalalgia* 28:1039–1047
8. Dodge FA Jr, Rahamimoff R (1967) Co-operative action of calcium ions in transmitter release at the neuromuscular junction. *J Physiol* 193:419–432
9. Dolphin AC (2003) G protein modulation of voltage-gated calcium channels. *Pharmacol Rev* 55:607–627
10. Drigo P, Carli G, Laverda AM (2000) Benign paroxysmal torticollis of infancy. *Brain Dev* 22:169–172
11. Dunn DW, Snyder CH (1976) Benign paroxysmal vertigo of childhood. *Am J Dis Child* 130:1099–1100
12. Evans RM, Zamponi GW (2006) Presynaptic Ca²⁺ channels— integration centers for neuronal signalling pathways. *Trends Neurosci* 29:617–624
13. Fernández-Fernández JM, Tomás M, Vázquez E, Orio P, Latorre R, Sentí M, Marrugat J, Valverde MA (2004) Gain-of-function mutation in the KCNMB1 potassium channel subunit is associated with low prevalence of diastolic hypertension. *J Clin Invest* 113:1032–1039
14. Forsythe ID, Tsujimoto T, Barnes-Davies M, Cuttle MF, Takahashi T (1998) Inactivation of presynaptic calcium current contributes to synaptic depression at a fast central synapse. *Neuron* 20:797–807
15. Giffin NJ, Benton S, Goadsby PJ (2002) Benign paroxysmal torticollis of infancy: four new cases and linkage to CACNA1A mutation. *Dev Med Child Neurol* 44:490–493
16. Hans M, Luvisetto S, Williams ME, Spagnolo M, Urrutia A, Tottene A, Brust PF, Johnson EC, Harpold MM, Stauderman KA, Pietrobon D (1999) Functional consequences of

- mutations in the human $\alpha 1A$ calcium channel subunit linked to familial hemiplegic migraine. *J Neurosci* 19:1610–1619
17. Hamill O, Marty A, Neher E, Sakmann B, Sigworth F (1981) Improved patch-clamp techniques for high-resolution current recording from cells and cell-free membrane patches. *Pflügers Arch* 391:85–100
 18. Jones LP, Patil PG, Snutch TP, Yue DT (1997) G-protein modulation of N-type calcium channel gating current in human embryonic kidney cells (HEK 293). *J Physiol* 498:601–610
 19. Kraus RL, Sinnegger MJ, Glossmann H, Hering S, Striessnig J (1998) Familial hemiplegic migraine mutations change $\alpha 1A$ Ca^{2+} channel kinetics. *J Biol Chem* 273:5586–5590
 20. Kraus RL, Sinnegger MJ, Koschak A, Glossmann H, Stenirri S, Carrera P, Striessnig J (2000) Three new familial hemiplegic migraine mutants affect P/Q-type Ca^{2+} channel kinetics. *J Biol Chem* 275:9239–9243
 21. Melliti K, Grabner M, Seabrook GR (2003) The familial hemiplegic migraine mutation R192Q reduces G-protein-mediated inhibition of P/Q-type ($CaV_{2.1}$) calcium channels expressed in human embryonic kidney cells. *J Physiol* 546:337–347
 22. Mori Y, Friedrich T, Kim MS, Mikami A, Nakai J, Ruth P, Bosse E, Hofmann F, Flockerzi V, Furuichi T, Mikoshiba K, Imoto K, Tanabe T, Numa S (1991) Primary structure and functional expression from complementary DNA of a brain calcium channel. *Nature* 350:398–402
 23. Müllner C, Broos LA, van den Maagdenberg AM, Striessnig J (2004) Familial hemiplegic migraine type 1 mutations K1336E, W1684R, and V1696I alter $CaV_{2.1}$ Ca^{2+} channel gating: evidence for β -subunit isoform-specific effects. *J Biol Chem* 279:51844–51850
 24. Neuhauser H, Lempert T (2004) Vertigo and dizziness related to migraine: a diagnostic challenge. *Cephalalgia* 24:83–91
 25. Pattillo JM, Artim DE, Simples JE Jr, Meriney SD (1999) Variations in onset of action potential broadening: effects on calcium current studied in chick ciliary ganglion neurones. *J Physiol* 514:719–728
 26. Pietrobon D (2007) Familial hemiplegic migraine. *Neurotherapeutics* 4:274–284
 27. Tombola F, Pathak MM, Isacoff EY (2006) How Does Voltage Open an Ion Channel? *Annu Rev Cell Dev Biol* 22:23–52
 28. Tottene A, Pivotto F, Fellin T, Cesetti T, van den Maagdenberg AM, Pietrobon D (2005) Specific kinetic alterations of human $CaV_{2.1}$ calcium channels produced by

mutation S218L causing familial hemiplegic migraine and delayed cerebral edema and coma after minor head trauma. *J Biol Chem* 280:17678–17686

29. van den Maagdenberg AM, Pietrobon D, Pizzorusso T, Kaja S, Broos LA, Cesetti T, van de Ven RC, Tottene A, van der Kaa J, Plomp JJ, Frants RR, Ferrari MD (2004) A *Cacna1a* knockin migraine mouse model with increased susceptibility to cortical spreading depression. *Neuron* 41:701–710
30. Weiss N, Sandoval A, Felix R, van den Maagdenberg A, De Waard M (2008) The S218L familial hemiplegic migraine mutation promotes deinhibition of CaV2.1 calcium channels during direct G-protein regulation. *Pflügers Arch* 457:315–326
31. Westenbroek RE, Sakurai T, Elliott EM, Hell JW, Starr TV, Snutch TP, Catterall WA (1995) Immunochemical identification and subcellular distribution of the α 1A subunits of brain calcium channels. *J Neurosci* 15:6403–6418

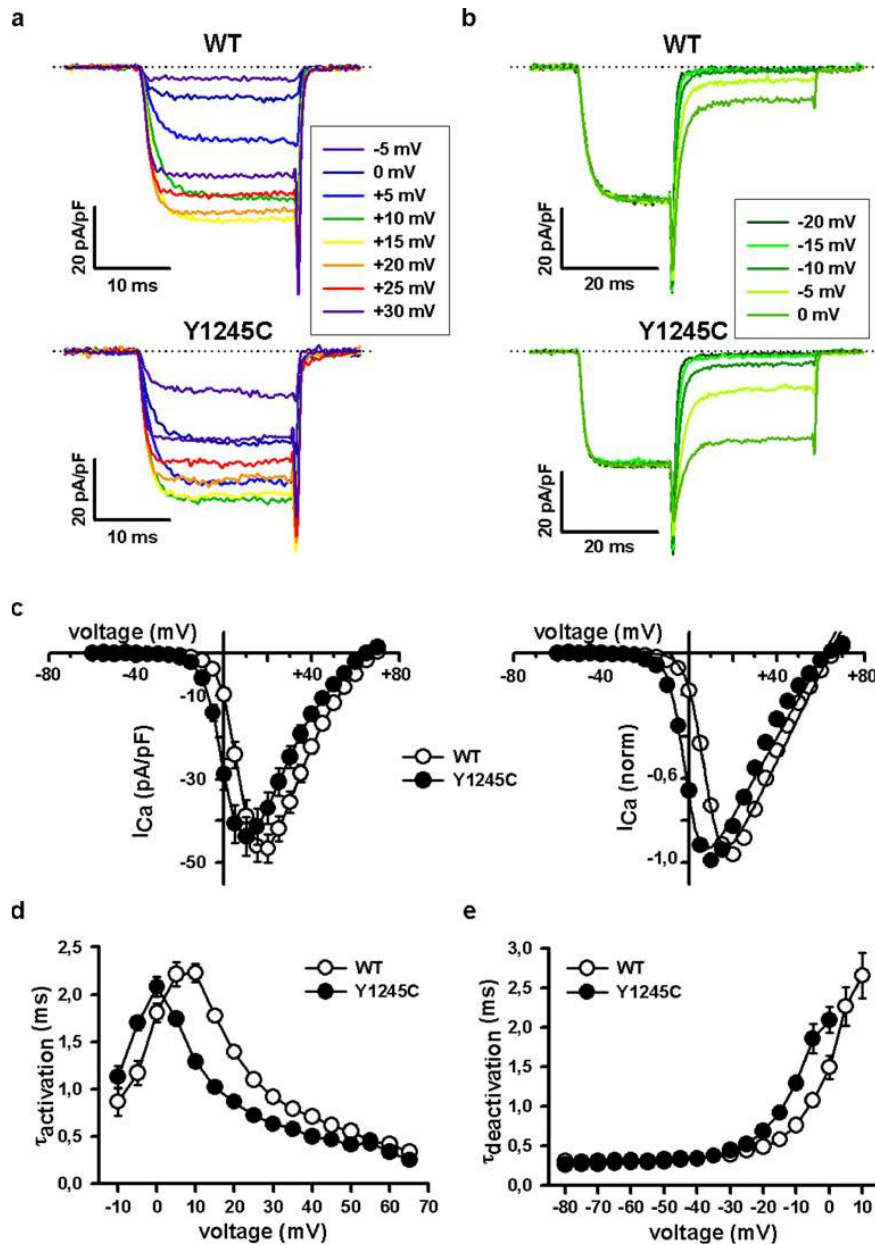


Fig. 2 Y1245C affects activation and deactivation properties of heterologously expressed P/Q channels. a Current traces illustrating voltage-dependence and activation kinetics of WT (top) and Y1245C (bottom) channels, in response to 20 ms voltage pulses. b Current traces illustrating deactivation kinetics of WT (top) and Y1245C (bottom) channels obtained by hyperpolarizing the cells during 30 ms at the indicated voltages following a 20-ms depolarizing pulse to +20 mV. Dotted lines in the current traces indicate the zero current level. c Current density- voltage relationships (left panels) and normalized I-V curves (right panels) for WT (empty circle, n=71) and Y1245C P/Q (filled circle, n=34) channels expressed in HEK 293 cells. $V_{1/2, act}$, k_{act} and V_{rev} values were (in mV): WT (empty circle, n= 71) 7.55 ± 0.44 , 3.93 ± 0.33 and 64.35 ± 0.83 ; Y1245C (filled circle, n=34) -1.48 ± 0.56 , 3.72 ± 0.44 and 61.56 ± 1.13 , respectively. Average τ_{act} d and τ_{deact} e of WT (empty circle) and Y1245C channels (filled circle) at the indicated voltages

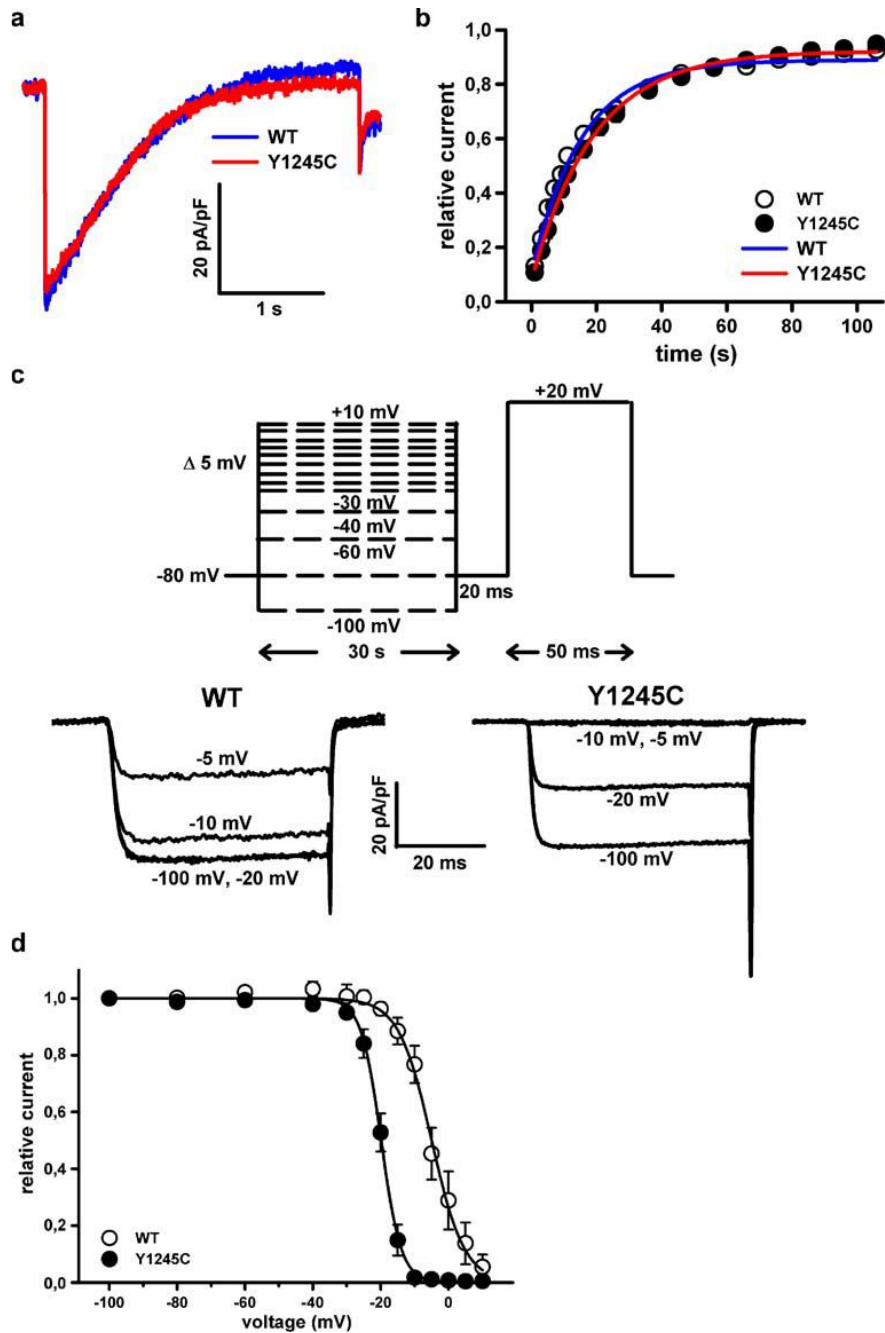


Fig. 3 Y1245C affects P/Q channel inactivation properties. a Current traces illustrating similar inactivation kinetics for WT (blue line, $\tau_{\text{inact}}=1.18 \pm 0.13$ s, $n=40$) and Y1245C (red line, $\tau_{\text{inact}}=0.92 \pm 0.13$ s, $n=27$) channels, in response to a 3 s depolarizing pulse to +20 mV. b Time course of I_{Ca} recovery from inactivation for WT and Y1245C channels. Average τ of current recovery from inactivation obtained after fitting the data to a single exponential, were (in seconds): WT (empty circle, $n=16$) 17.16 ± 1.91 ; Y1245C (filled circle, $n=23$) 19 ± 1.85 . c and d Steady-state inactivation (voltage protocol on top) of WT or Y1245C P/Q channels. Amplitudes of currents elicited by test pulses to +20 mV were normalized to the current obtained after a 30-s prepulse to -100 mV and fitted by a single Boltzmann function (see “Materials and methods”, Eq. 2). $V_{1/2, \text{inact}}$ and k_{inact} values were (in mV): WT (empty circle, $n=14$) -4.96 ± 0.6 and -4.83 ± 0.57 ; Y1245C (filled circle, $n=10$) -19.85 ± 0.25 and -2.97 ± 0.23 , respectively

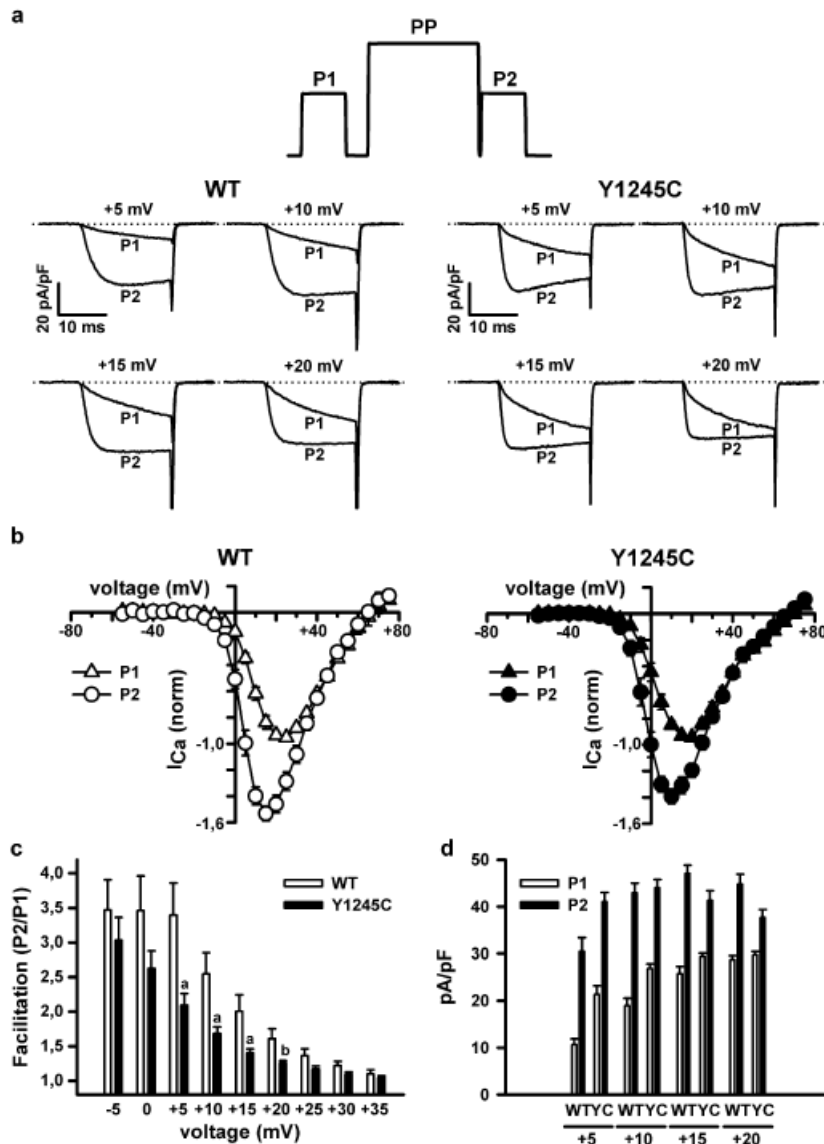


Fig. 4

Comparative G $\beta\gamma$ -mediated inhibition of WT and Y1245C P/ Q channels. a WT (left) or Y1245C (right) currents recorded at the indicated voltages before (P1) and after (P2) a 50 ms conditioning prepulse to +100 mV (PP) in the presence of G β 1 γ 2. Currents are superposed to facilitate comparison. Dotted lines mark the zero current level. b I-V relationships for WT (left, P1 (empty upright triangle) and P2 (empty circle)) and Y1245C (right, P1 (filled upright triangle) and P2 (filled circle)) channels in the presence of G β 1 γ 2 subunits. Currents were normalized to the maximal current amplitude before the prepulse and then averaged. V_{1/2}, act, kact and V_{rev} values were (in mV): WT P1 (empty upright triangle, n=14) 10.33±0.38, 4.8±0.28 and 67.32±0.56; WT P2 (empty circle, n=14) 3.95±0.55, 3.65±0.43 and 64.59±1.02; Y1245C P1 (filled upright triangle, n=14) 3.07± 0.53, 4.91±0.4 and 67.84±0.92; Y1245C P2 (filled circle, n=14) -2.38±0.62, 3.87±0.49 and 64.41±1.23, respectively. c Mean current amplitude facilitation (P2/P1 ratio) plotted against test potential for WT (n=14) and Y1245C (n=14) P/Q channels in the presence of G β 1 γ 2 (aP<0.01, bP<0.05). d Mean current density at the indicated test voltages for WT (n=14) and Y1245C (n=14) P/Q channels in the presence of G β 1 γ 2 before (P1) and after (P2) a 50-ms conditioning prepulse to +100 mV. ICa inhibition (in %) by G β 1 γ 2 for WT and Y1245C channels estimated from P1 and P2 current densities: @ +5 mV, 64.63±3.99 (WT) and 47.16±5.06 (Y1245C) (P<0.01); @ +10 mV, 55.13±4.1 (WT) and 37.36±4.21 (Y1245C) (P<0.01); @ +15 mV, 43.83±4.51 (WT) and 27.15±3.16 (Y1245C) (P<0.01); @ +20 mV, 33.55±4.13 (WT) and 20.03±2.27 (Y1245C) (P<0.05)

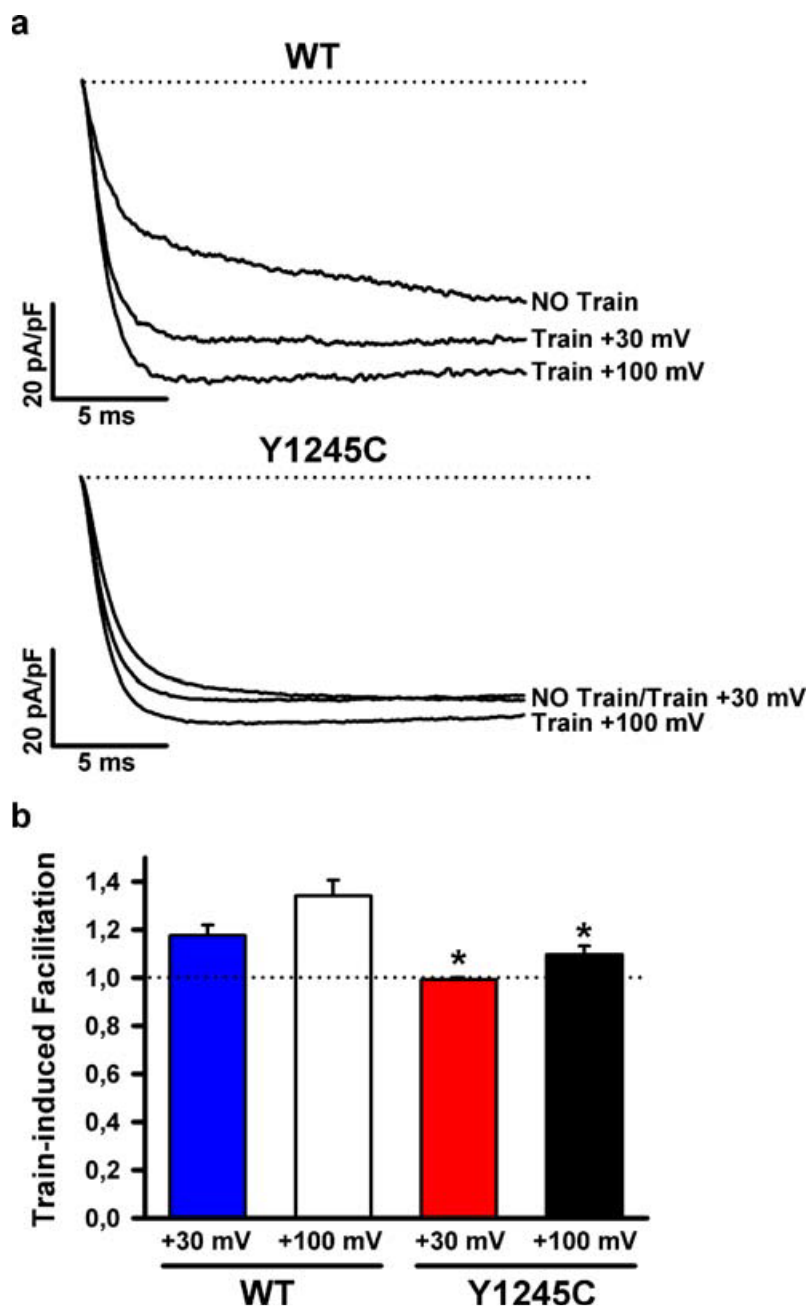


Fig. 5 Y1245C reduces P/Q current facilitation in response to a train of depolarizing pulses. a WT (top) or Y1245C (bottom) Ca²⁺ currents recorded in the presence of G β 1 γ 2 at +20 mV before (NO Train) and 1 ms after conditioning the cell with a train of 15 short (4 ms) depolarizing pulses to +30 mV or +100 mV (as indicated), delivered at 71.4 Hz. Currents are superposed to facilitate comparison. Dotted lines show the zero current level. b Mean current amplitude facilitation (P₂/P₁ ratio) plotted against train potential for WT (n=4) and Y1245C (n=6) P/Q channels in the presence of G β 1 γ 2 (*P<0.01). In this set of experiments, maximal I_{Ca} facilitation @ +20 mV induced by a 50 ms prepulse to +100 mV was 1.7±0.18 for WT channels and 1.24±0.07 for Y1245C channels (P<0.05)

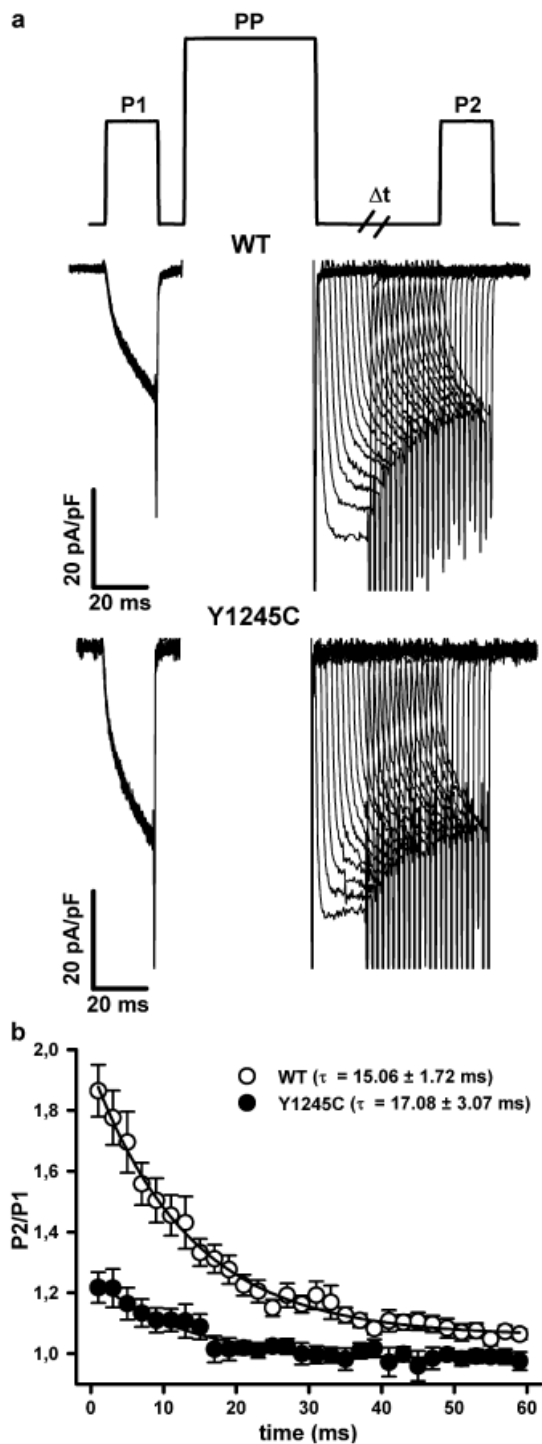


Fig. 6 Similar kinetics of facilitation decay for WT and Y1245C P/Q channels. a Representative examples of re-inhibition by $G\beta 1\gamma 2$ (facilitation decay) of ICa through WT and Y1245C channels, as indicated. Ca^{2+} currents were evoked by using the three-voltage-step protocol illustrated ($\Delta t=2$ ms; see “Materials and methods” for details). b Average facilitation decay kinetics for WT (empty circle, $n=27$) and Y1245C (filled circle, $n=6$) channels as a function of interpulse duration at -80 mV. Mean time constants (in ms) of re-inhibition ($G\beta 1\gamma 2$ re-association to the channel) were 15.06 ± 1.72 for WT and 17.08 ± 3.07 for Y1245C channels ($P=0.61$). In this set of experiments, maximal ICa facilitation @ $+20$ mV was 1.86 ± 0.08 for WT and 1.22 ± 0.05 for Y1245C ($P<0.01$)

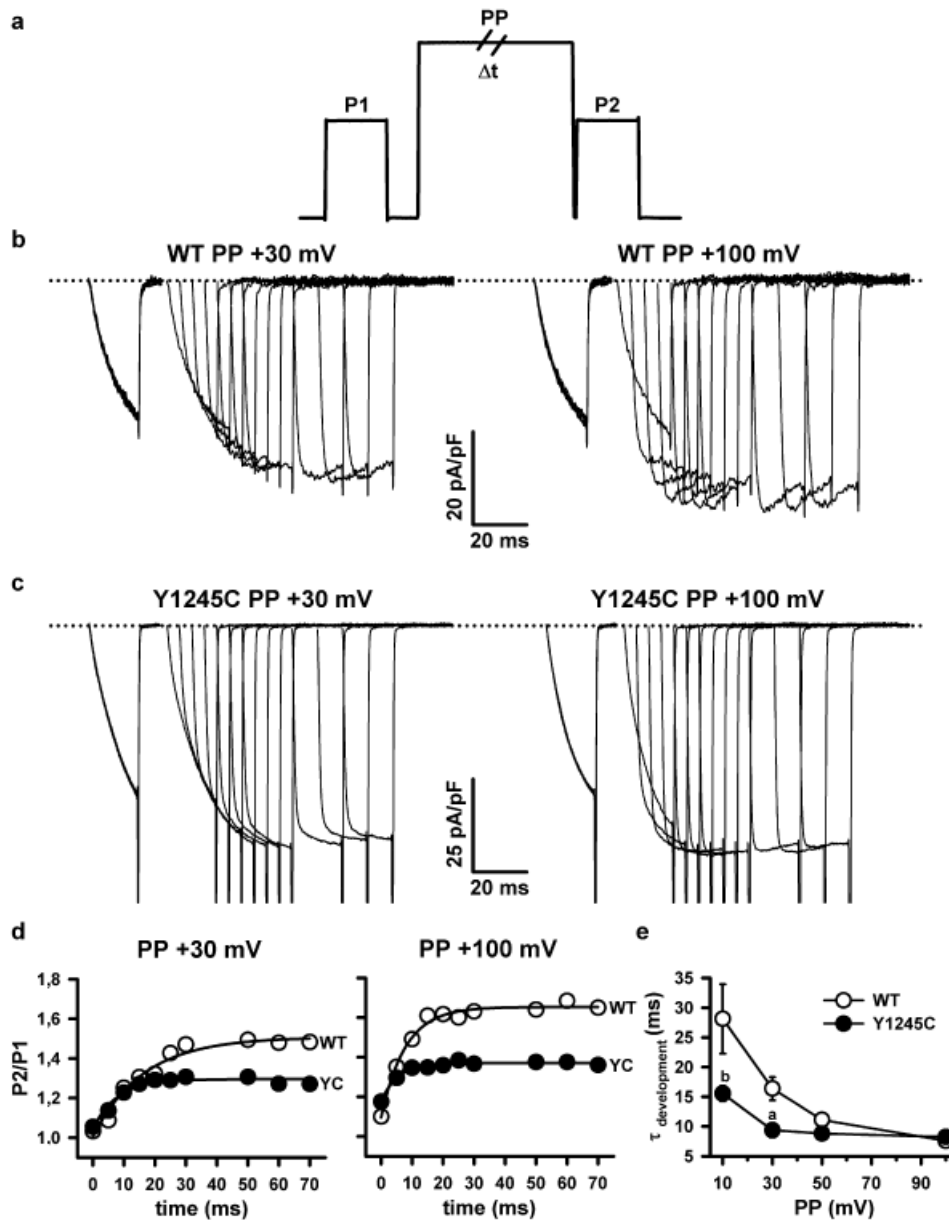


Fig. 7 Y1245C accelerates the apparent rate of $G\beta\gamma$ dissociation from P/Q channels at low depolarizing voltages. Representative examples of relief of $G\beta_1\gamma_2$ block (facilitation development) for WT (b) and Y1245C (c) channels measured at +30 (left) and +100 (right) mV prepulse (PP), as indicated, and the corresponding time course of facilitation development, as a function of facilitatory prepulse duration (empty circle WT and filled circle; Y1245C; d). Ca^{2+} currents were evoked by using the three-voltage-step protocol illustrated in (a) (see “Materials and methods” for details). Dotted lines in the current traces denote the zero current level. e Average time constant (in ms) of facilitation development, $G\beta_1\gamma_2$ dissociation from the channel, for WT (empty circle $n=6-34$) and Y1245C (filled circle $n=5-16$) channels at the indicated PP voltages ($aP<0.01$, $bP<0.05$). In this set of experiments, maximal ICa facilitation @ +20 mV was 1.31 ± 0.04 ; 1.68 ± 0.14 ; 1.88 ± 0.23 ; and 1.77 ± 0.08 , for WT channels; and 1.2 ± 0.04 ; 1.26 ± 0.06 ; 1.25 ± 0.06 and 1.33 ± 0.06 , for Y1245C channels, when applying 70 ms prepulses of +10 ($P=0.09$), +30 ($P<0.01$), +50 ($P<0.05$), and +100 mV ($P<0.001$), respectively

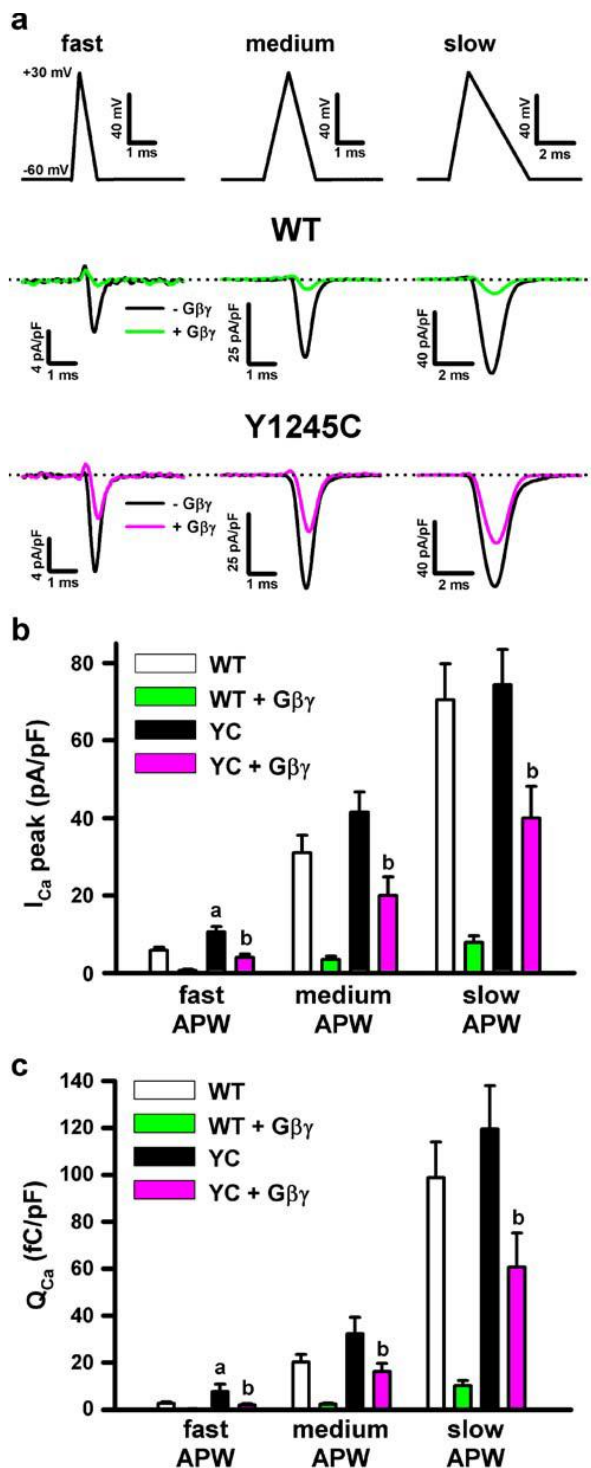


Fig. 8 Y1245C lessens Gβγ-induced inhibition of calcium influx evoked by action-potential-like waveforms (APWs). a Representative Ca²⁺ current traces evoked by APWs of different durations (fast (left panels), medium (central panels) and slow (right panels; see “Materials and methods” for details) obtained from HEK 293 cells expressing WT (top) or Y1245C (bottom) P/Q channels in the absence (-Gβγ) or presence (+Gβγ) of Gβ1γ2 dimers. Dotted lines stand for the zero current level. Averaged data for peak current density (b) and normalized Ca²⁺ influx (Q_{Ca}) (c) in response to the above-mentioned APWs obtained from cells expressing WT (n=7-10) or Y1245C (n=8-9) P/Q channels in the absence (-Gβγ, n=9-10) or presence (+Gβγ, n=7-8) of Gβ1γ2 dimers, as indicated (aP<0.01 versus WT, bP<0.01 versus WT+Gβγ). In this series of experiments, extracellular [Ca²⁺] was 5 mM

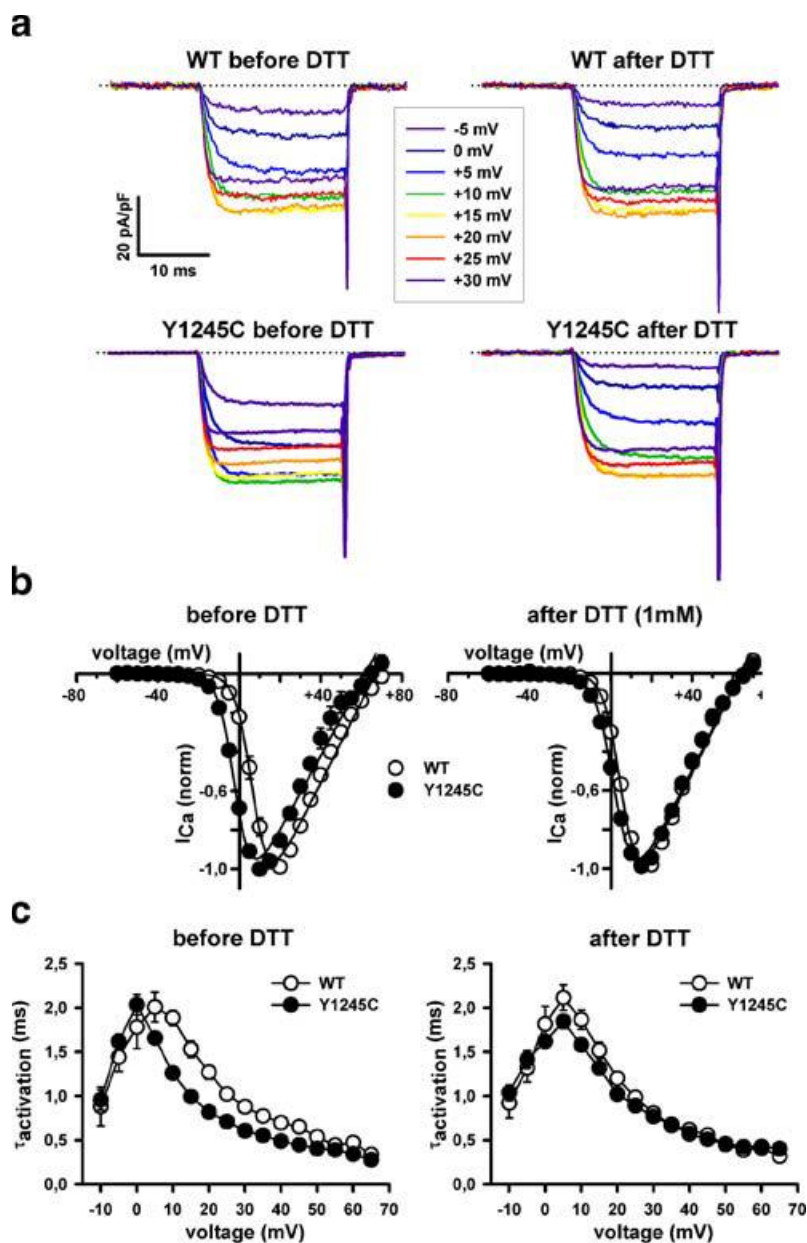


Fig. 9 DTT minimizes the effect of Y1245C on voltage-dependency and kinetics of P/Q channel activation. a Current traces of WT (top) and Y1245C (bottom) channels, in response to 20 ms depolarizing pulses at the indicated voltages, before (left) and 5 min after (right) exposure to 1 mM DTT. The zero current level is indicated by the dotted lines. (b) Normalized I-V curves for WT and Y1245C P/Q channels expressed in HEK 293 cells before (left) and after (right) exposure to 1 mM DTT. $V_{1/2, act}$, t_{act} , and V_{rev} values were (in mV): WT before DTT (empty circle $n=10$) 6.95 ± 0.38 , 4.09 ± 0.29 , and 67.04 ± 0.8 ; Y1245C before DTT (filled circle, $n=17$) -1.68 ± 0.58 , 4.04 ± 0.45 , and 61.93 ± 1.11 ; WT after DTT (empty circle, $n=10$) 5.59 ± 0.43 , 4.16 ± 0.32 , and 63.62 ± 0.77 ; Y1245C after DTT (filled circle, $n=17$) 2.55 ± 0.44 , 4.71 ± 0.32 , and 63.83 ± 0.75 , respectively. c Average τ_{act} of WT (empty circle) and Y1245C channels (filled circle) at the indicated voltages, before (left) and after (right) exposure to 1 mM DTT

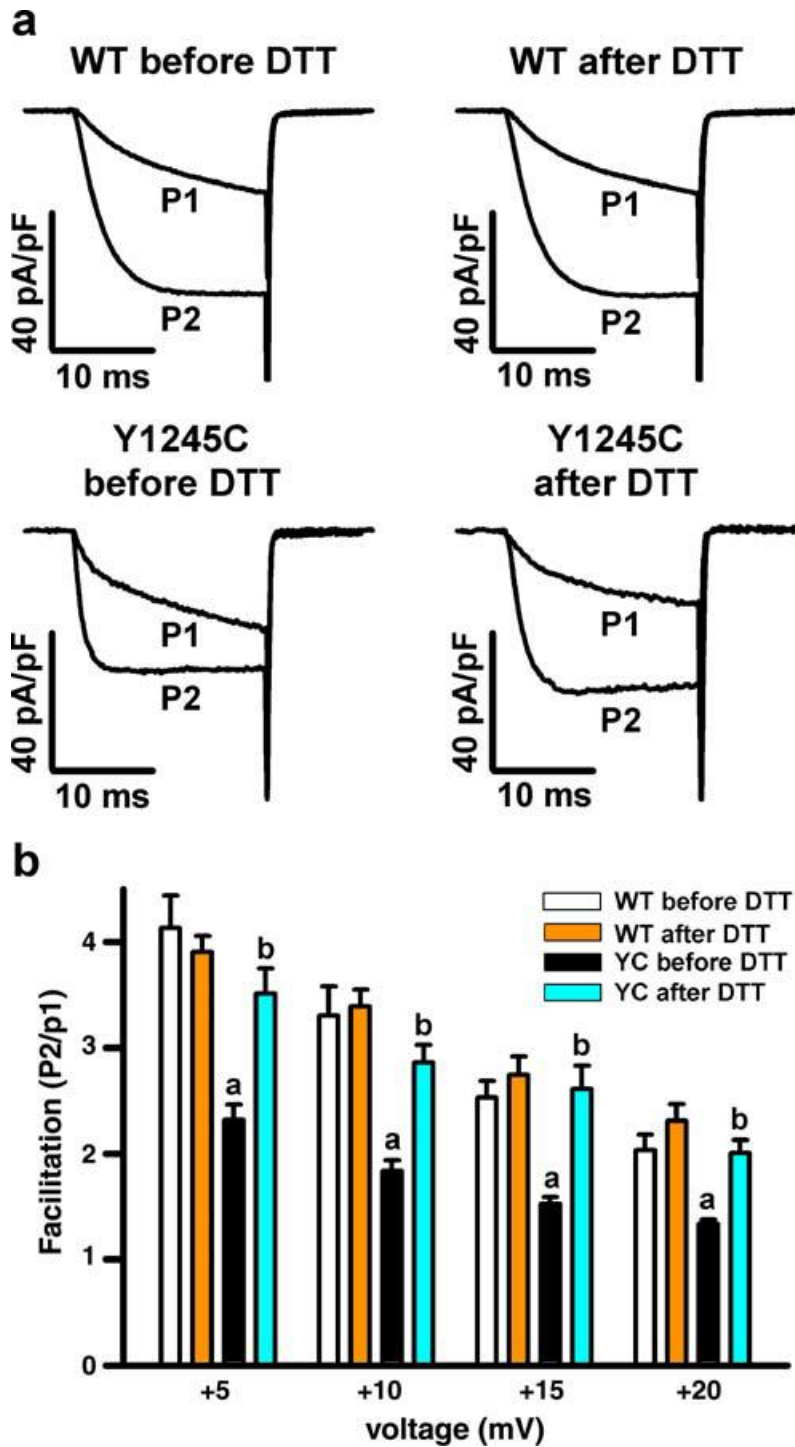


Fig. 10 DTT reverses the effect of Y1245C on $G\beta\gamma$ -mediated inhibition of P/Q channels. **a** WT (top) or Y1245C (bottom) P/Q currents elicited by a test pulse to +15 mV before (P1) and following (P2) a 50-ms conditioning prepulse to +100 mV in the presence of $G\beta_1\gamma_2$, prior to (left) and 5 min after (right) exposure to 1 mM DTT. Currents are superposed to facilitate comparison. **b** Mean current amplitude facilitation (P2/P1 ratio) versus test potential for WT ($n=9$) and Y1245C ($n=6$) P/Q channels in the presence of $G\beta_1\gamma_2$, before and after exposure to DTT, as indicated (a $P<0.01$ versus WT before DTT, b $P<0.05$ versus YC before DTT)